Quantification and Predictors of OCT-Based Macular Curvature and Dome-Shaped Configuration: Results From the UK Biobank

Philipp L. Müller,[1–4] Yuka Kihara,[5] Abraham Olvera-Barrios,[1,2] Alasdair N. Warwick,[1,6] Catherine Egan,[1,2] Katie M. Williams,[1,2,7] Aaron Y. Lee,[5] and Adnan Tufail[1,2]; for the UK Biobank Eyes and Vision Consortium

[1]Moorfields Eye Hospital NHS Foundation Trust, London, United Kingdom
[2]Institute of Ophthalmology, University College London, London, United Kingdom
[3]Macula Center, Südblick Eye Centers, Augsburg, Germany
[4]Department of Ophthalmology, University of Bonn, Bonn, Germany
[5]Department of Ophthalmology, University of Washington, Seattle, Washington, United States
[6]Institute of Cardiovascular Science, University College London, London, United Kingdom
[7]Section of Academic Ophthalmology, School of Life Course Sciences, FoLSM, King's College London, United Kingdom

Correspondence: Adnan Tufail, Moorfields Eye Hospital NHS Foundation Trust, 162 City Road, London EC1V 2PD, UK; adnan.tufail@nhs.net.

PLM and YK contributed equally to the work presented here and should therefore be regarded as equivalent authors.
The UKBB Eyes and Vision Consortium is available online at www.aaojournal.org.

Received: March 24, 2022
Accepted: July 11, 2022
Published: August 25, 2022

Citation: Müller PL, Kihara Y, Olvera-Barrios A, et al. Quantification and predictors of OCT-based macular curvature and dome-shaped configuration: Results from the UK Biobank. *Invest Ophthalmol Vis Sci.* 2022;63(9):28. https://doi.org/10.1167/iovs.63.9.28

Purpose. To investigate macular curvature, including the evaluation of potential associations and the dome-shaped macular configuration, given the increasing myopia prevalence and expected associated macular malformations.

Methods. The study included a total of 65,440 subjects with a mean age (± SD) of 57.3 ± 8.11 years with spectral-domain optical coherence tomography (OCT) data from a unique contemporary resource for the study of health and disease that recruited more than half a million people in the United Kingdom (UK Biobank). A deep learning model was used to segment the retinal pigment epithelium. The macular curvature of the OCT scans was calculated by polynomial fit and evaluated. Further, associations with demographic, functional, ocular, and infancy factors were examined.

Results. The overall macular curvature values followed a Gaussian distribution with high inter-eye agreement. Although all of the investigated parameters, except maternal smoking, were associated with the curvature in a multilinear analysis, ethnicity and refractive error consistently revealed the most significant effect. The prevalence of a macular dome-shaped configuration was 4.8% overall, most commonly in Chinese subjects as well as hypermetropic eyes. An increasing frequency up to 22.0% was found toward high refractive error. Subretinal fluid was rarely found in these eyes.

Conclusions. Macular curvature revealed associations with demographic, functional, ocular, and infancy factors, as well as increasing prevalence of a dome-shaped macular configuration in high refractive error including high myopia and hypermetropia. These findings imply different pathophysiologic processes that lead to macular development and might open new fields to future myopia and macula research.

Keywords: retina, OCT, artificial intelligence, deep learning, refraction

It is commonly believed that the retina follows the roundness of the globe and shows a slight outward directed curve. Nevertheless, divergent macular configurations such as staphyloma or a dome-shaped macular configuration have been described.[1–4] These divergent configurations are reported to be mainly associated with such features as thickened sclera and choroid in the context of or secondary to high myopia (apart from space-occupying processes such as choroidal tumors),[5] defined by refractive error exceeding −6 diopters (D) or axial length of ≥26 mm.[1–4,6] In the cohort with high myopia, it was reported with a frequency of 4% to 15%.[1,2] Given the increasing myopia prevalence,[7,8] understanding macula malformation in the context of myopia is vital, as it is a strong driver of maculopathy development is the presence of a posterior staphyloma with anomalous macula curvature.[7,9,10] However, myopia research is dominated by exploring associations of refractive error or occasionally axial length, but not macula curve, due to difficulty measuring it. Therefore, the pathophysiology underlying macular malformations, especially dome-shaped maculopathy, is not completely understood nor has the prevalence of these malformations been systematically investigated.

In the last decade, high-definition optical coherence tomography (OCT) has become widely available that allows for three-dimensional imaging of the macula.[11] In this context, objective quantification of the macular curvature

has recently been introduced.[12] It might offer the potential for an effective comprehensive evaluation. Although macular curvature has been reported to be associated with choroidal thickness and axial length, as well as retinitis pigmentosa and associated genes,[12–15] large epidemiologic studies are still pending.

With over 500,000 recruited adults, UK Biobank (UKBB) is the world's largest single resource for the study of health and disease.[16–18] A subset of subjects underwent enhanced ophthalmic examinations that included obtaining OCT data.[19] This study, therefore, used this unique opportunity to comprehensively and systematically investigate macular curvature—in particular, the prevalence of the dome-shaped configuration in the UKBB—and to evaluate potential associations that can be tested in later studies. Further insights into macular configurations and development might be of particular scientific interest for myopia research, the study of ocular development, and to investigate the many ocular diseases associated with this particular region, including age-related macular degeneration, the most common cause of legal blindness in the developed world.[20]

Methods

Study Populations

Between 2006 and 2010, the UKBB study recruited 502,682 subjects who were between 40 and 69 years of age, registered with the UK National Health Service (NHS), and living within a 25-mile radius of one of the 22 study assessment centers. The study was approved by the National Information Governance Board for Health and Social Care and the NHS North West Multicenter Research Ethics Committee (reference no. 06/MRE08/65), and was conducted in accordance with the tenets of the Declaration of Helsinki.[18,19,21] Detailed information and study protocols are available online at the UKBB website (www.ukbiobank.ac.uk). This research has been conducted using the UK Biobank Resource under application number 60554.

Enhanced ophthalmic assessments were attended by 133,630 participants and included measures of refractive error, autorefraction, visual acuity (VA), and intraocular pressure (IOP); 85,737 subjects had macular spectral-domain OCT imaging performed at six UKBB centers (Sheffield, Liverpool, Hounslow, Croydon, Birmingham, and Swansea) that was used for further analysis. Participants with prior refractive laser or surgery, OCT data inappropriate for polynomial fit (e.g., insufficient quality, dealignment), and missing or incomplete associated data were excluded from further analysis (Fig. 1). In line with the UKBB, our study did not exclude eyes with known ocular diseases, as we aimed to present a representative cross-section of the studied population. Emmetropia (−1 to +1 D), hypermetropia (>+1 D), and myopia (<−1 D) were defined based on refractive error (spherical equivalent). Further subclassifications were made into mild (>+1 to +3 D and −3 to <−1 D), moderate (>+3 to +6 D and −6 to <−3 D), or high (>+6 D and <−6 D) hypermetropia and myopia, respectively.

Imaging

A 6 × 6-mm^2 macular OCT volume scan (128 B-scans with 512 A-scans each) was performed using a spectral-domain OCT imaging device (3D OCT-1000 Mark II; Topcon, Tokyo, Japan) in a dark room without pupil dilatation. The right eye was imaged first. The scan was then repeated for the left eye. The horizontal raster scans from the OCT device used in the

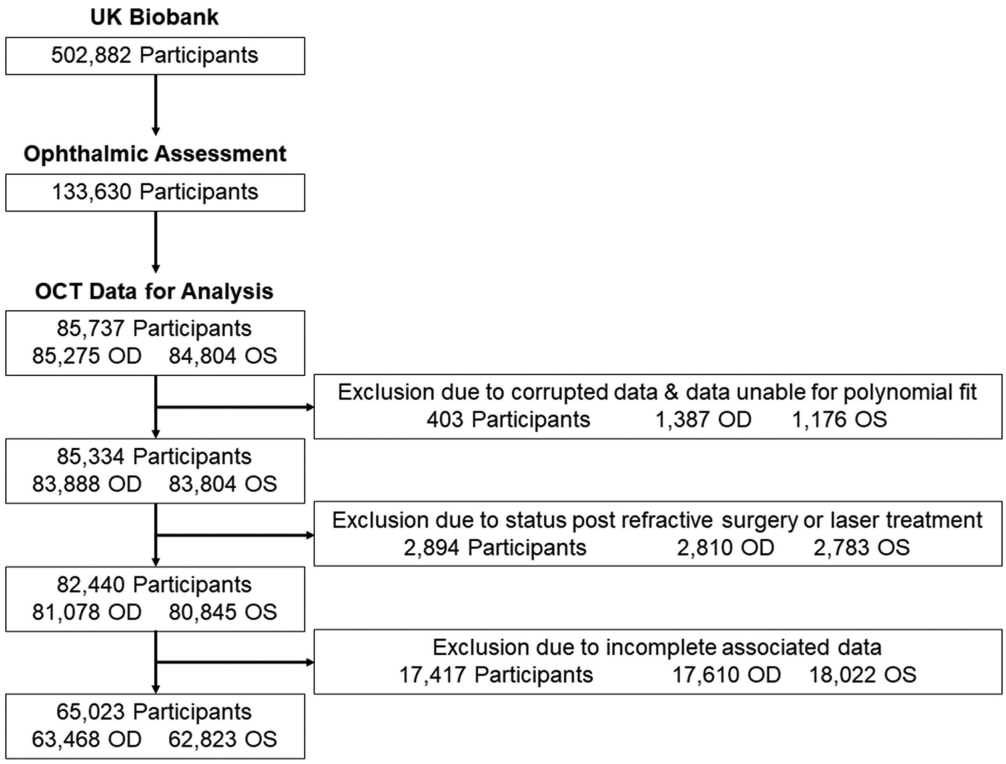

Figure 1. Inclusion and exclusion of subjects. The flow chart demonstrates the selection of the study population.

UKBB (Topcon 3D OCT-1000) did not undergo any sort of spatial processing that would alter the curvature (personal communication with Topcon Research). However, varying optical path distortions by OCT system optics or relative eye positions could not be excluded.[22] The OCT data were stored as FDS files, a proprietary image storage file format, on the UKBB supercomputers in Oxford, UK, without prior analysis.

Curvature Analysis

Our aim was to build a machine learning model that can extract the area between the inner limiting membrane and retinal pigment epithelium (RPE) from OCT B-scans and thus detect the boundary of the RPE and choroid (RPE/C) without any human annotations (Supplementary Fig. S1). For this, the FDS files were transformed into FDA data. Then, we first employed the A* (A_star) algorithm to obtain initial segmentation masks of the retinal layers,[23] and we used them as the initial training target for the machine learning model. The A* algorithm is an extension of Edsger Dijkstra's algorithm, which is widely used in pathfinding and graph traversal,[24] and thus can be adopted to distinguish different parts of boundaries in graph-based image segmentation problems. However, this traditional image segmentation algorithm is not robust enough to handle images with poor contrast or abnormal brightness filled with random noise; in fact, the output segmentation masks included many errors. In order to filter out these errors, we calculated the minimum retinal thickness and standard deviation (SD) for each B-scan from predicted segmentation masks. In this study, only the samples with a minimal retinal thickness between 30 and 80 pixels (which converts to 180 to 480 µm at an axial resolution of 6 µm/pixel) and SD $\leq$ 10 pixels (60 µm) were accepted. We processed one B-scan from randomly selected 8500 FDA data.

Through the process described above, we collected a total of 6409 input–output pairs. We used the Pyramid Parsing Network (PSPNet) with the ResNet18 backbone as our segmentation architecture.[25,26] The model was trained with a binary cross-entropy loss function using the Adam optimizer. We chose a batch size of 8. The learning rate was initially set to 1×10^{-3}, and decay over each update was set to initial learning ratio divided by epochs. All inputs and outputs were cropped to 512 $\times$ 512 by setting y-coordinates whose sum of pixel values had a maximum intensity to the center and then resized to 256 $\times$ 256. All images were normalized to a range between 0 and 1. We assessed the performance of the neural network using cross-validation with the validation set and evaluated the generalizability with an independent dataset. Samples were divided into training sets at 80%, validation sets at 20%. The training and validation sets contained images from mutually exclusive groups of subjects. During the training, shadows and Gaussian/speckle noises were randomly applied to the training data, as well as basic data augmentations such as shift, flip, and rotation.

When we filtered out segmentation errors from the A* algorithm, many hard examples were also excluded from the dataset; therefore, the trained model was not robust enough at this point. In order to bolster this weakness, we retrained our model with additional hard examples. For this, we first processed 1250 FDA data items and excluded segmentation error. Next, we computed a sum of entropy for each obtained segmentation mask where each pixel had a probability value of being foreground. We then regarded examples with high entropy value as hard examples, which were sorted in descending order, and the top 200 images were added to the original dataset for the training. The model achieved a mean intersection over union value of 0.97 on the validation set.

In the end, a total of 170,079 eye images were processed and 128 $\times$ 170,079 segmentation masks were generated by the segmentation network. Because the B-scans often include several vertically flipped images, we built a binary classification network with the LeNet architecture that can identify flipped B-scans and unflip them automatically.[27] RPE/C boundaries were then extracted simply by tracking the bottom boundary for each segmentation mask. For each extracted RPE/C boundary, a two-dimensional polynomial curve was fitted at the center 32 slices of B-scans, separately. In the absence of axial length data or data for the OCT device optics, a correction for distortions by different lateral scaling or varying optical paths was not possible.[22,28,29] Finally, the median of coefficients of the leading term was saved as a representative curvature value of the eye (Supplementary Fig. S1).

Validation of Curvature Analysis

In order to validate the macular curvature analysis, the eyes were divided into quartiles based on macular curvature values. Randomly (using the True Random Number Generator, https://www.random.org/), one eye of each quartile was chosen and the central OCT scan was included in an Adobe PhotoShop PSD file (Fig. 2). Ten PSD files consisting of one OCT scan per quartile were generated. The files were saved twice: once with layers in random order for validation and once with the correct order of layers as control. Two independent experienced retinal specialists (P.L.M. and A.T.), masked to the results of the other, were then asked to order the four OCT scans in each PSD file (random order) according to the appearance of macular curvature. Finally, the results were compared to the control files, which revealed perfect agreement. Furthermore, the 100 cases with the most extensive curvature values were manually checked.

Statistical Analysis

Statistical analysis was performed using R 4.0.3 (R Foundation for Statistical Computing, Vienna, Austria) and Python 3.7 (Python Software Foundation, Wilmington, DE, USA). The distribution of the macular curvature and its correlation with ethnicity (white, comprised of English/Irish or other white background; Asian, comprised of British Asian, Indian, Pakistani, Bangladeshi, or other Asian background; black, comprised of black British, Caribbean, African, or other black background; Chinese; mixed, comprised of white and black Caribbean or African, white and Asian, or other mixed background; and other, comprised of undefined ethnicity), demographic, ocular, and functional parameters were investigated. These parameters included refractive error, as spherical equivalent (D), measured by autorefractor and calculated as sphere + [cylinder/2]); VA (in logarithm of the minimum angle of resolution [logMAR]); corneal-corrected IOP (mmHg), measured using the Ocular Response Analyzer (Reichert Corp., Buffalo, USA); age; sex; corneal curvature, measured as maximal curvature (K_{MAX}); childhood environment (birth weight, maternal smoking); and fluid intelligence (FI) score based on a baseline touchscreen questionnaire with 13 questions. Factors were chosen according

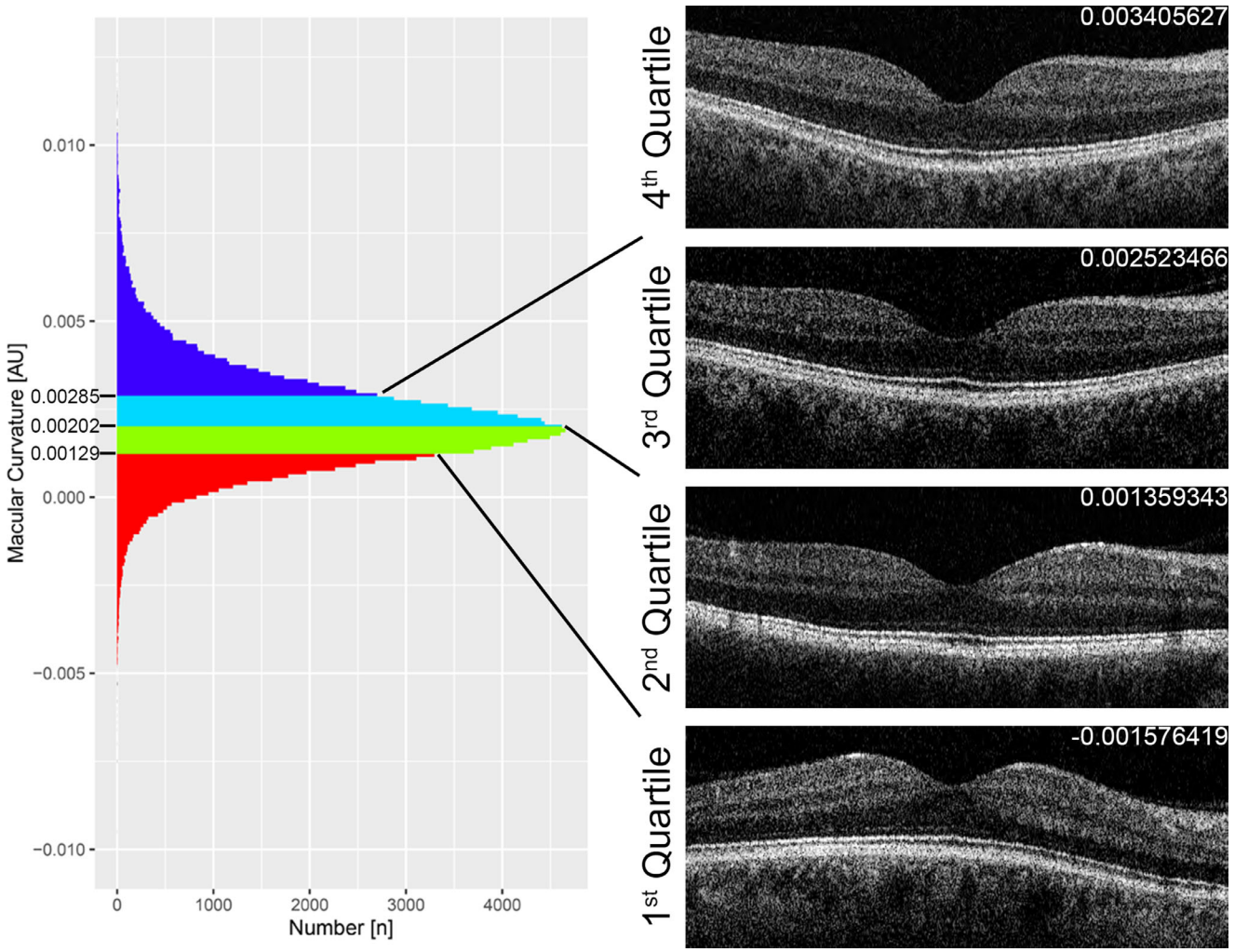

Figure 2. The spectrum of macular curvature. The histogram (*left*) shows the distribution of macular curvature values; the *colors* highlight the four different quartiles. The optical coherence tomography B-scans (*right*) represent exemplary images for all four quartiles as used for validation. For the demonstrated exemplary set, the individual curvature value of the respective eyes is displayed. The *bottom* image shows an inward-directed macular curve associated with a negative curvature value, indicating a dome-shaped configuration.

to literature evaluations, as associations with eye development or effects on the pathogenesis of dome-shaped macular curvature have been hypothesized. [1,4,30–35]

Multilevel linear regression models adjusting for age, gender, and ethnicity (demographic parameters) as fixed effects, with a random effect for person to allow for the right- and left-eye data from the same person to contribute to the analysis (model 1), were used to examine associations with macular curvature. Model 2 extended model 1 with further adjustment for ocular measures (refractive error, IOP, corneal curvature) and functional data (VA, FI). Model 3 extended model 2 with further adjustment for childhood environment (birth weight, maternal smoking). Macular curvature measures were modeled as *z*-scores in the regression models, and coefficients represent the fraction of SD change per unit increase or per group change (for categorical values) in covariates. Age represents the changes per decade increase, VA per 0.1 logMAR change, and IOP per 5-mmHg rise; other continuous variables are expressed in their units. References for categorical variables are female versus male, white versus all other ethnicities, and maternal smoking versus no maternal smoking. For inter-eye comparisons, paired *t*-tests were used. *P* values with $\alpha < 0.05$ were considered statistically significant.

Results

A total of 126,291 eyes of 65,023 subjects (35,176 female) with a mean age ± SD of 57.3 ± 8.11 years were included. The vast majority were assigned to white ethnicity (90.4% of included participants). In terms of refractive error, 58,432 eyes of 34,813 subjects (46.3%) were emmetropic; 33,283 eyes of 20,007 subjects (26.4%) were hypermetropic, with 25,843 eyes (16,769 subjects), 6317 eyes (4494 subjects), and 1123 eyes (828 subjects) assigned to mild, moderate, and high hypermetropia, respectively. Also, 34,576 eyes (27.4%) of 20,205 subjects were myopic with 17,278 eyes (11,986 subjects), 12,355 eyes (8139 subjects), and 4943 eyes (3322 subjects) assigned to mild, moderate, and high myopia, respectively (Supplementary Fig. S2). Further demographic, morphologic and functional parameters can be found in Supplementary Table S1.

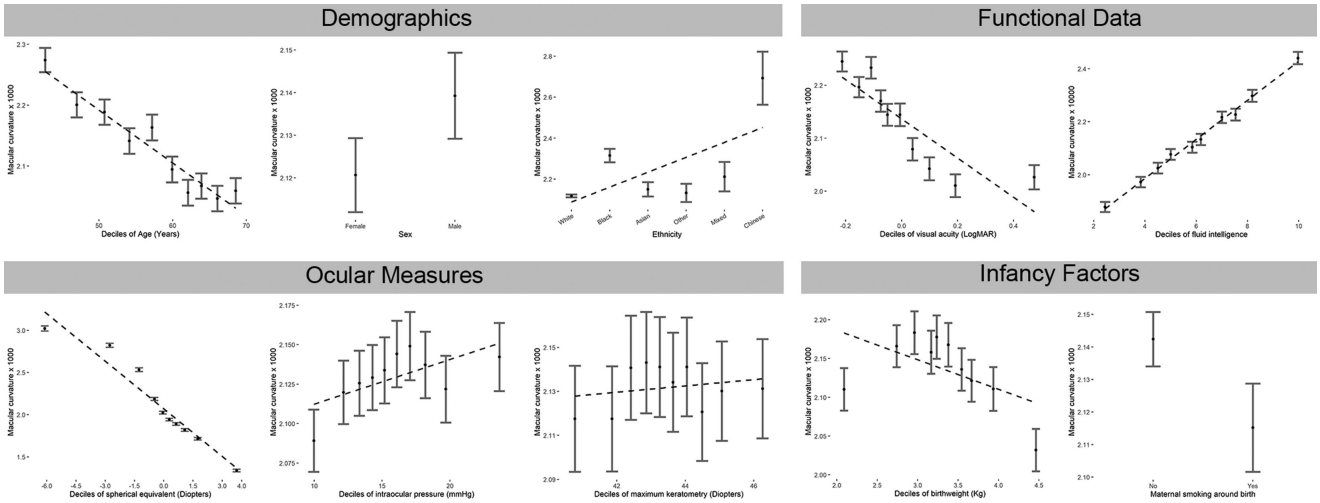

Figure 3. Macular curvature and associated parameters. The panel reveals adjusted mean macular curvature by deciles of variables of interest. Adjusted means (*solid black dots*), 95% confidence intervals (*vertical solid lines*), and regression lines (*dotted line*) are from a multilevel model allowing for repeated macular curvature measurement for each person.

Association with Macular Curvature

The overall macular curvature described a Gaussian distribution with a mean (± SD) of 0.00213 ± 0.00145 (Fig. 2). Multiple putative associated features of macular curvature were initially considered, including demographic characteristics (age, ethnicity, sex), ocular measures (refractive error, IOP, corneal curvature), functional data (VA, FI), and childhood environment (birth weight, maternal smoking). Figure 3 shows the association of macular curvature with each explored covariate. Here, as well as in a linear regression analysis, refractive error indicated the most distinct correlation ($r = -0.391$, $P > 0.001$), revealing lower macular curve values (i.e., flatter curve) with increasing spherical equivalent. Associations of other parameters with macular curvature were lower but evident (Fig. 3). Maternal smoking during pregnancy (mean = 0.00212) and female sex (mean = 0.00212) were associated with a slightly lower macular curvature (maternal non-smoking, mean = 0.00214; males, mean = 0.00214). Concerning ethnicity, white subjects (mean = 0.00212 ± 0.00145) and Asian subjects (mean = 0.00215 ± 0.00132) showed the lowest macular curvature, whereas Chinese subjects (mean = 0.00272 ± 0.00192) and black subjects (mean = 0.00235 ± 0.00127) revealed the highest overall values (Fig. 3). Of note, white participants (mean = −0.30 ± 2.71 D) and Chinese participants (mean = −2.26 ± 3.19 D) also represented the subgroups in terms of lowest and highest refractive errors, respectively. However, the black subgroup also revealed low refractive error (mean = −0.39 ± 2.25 D), in the range of white subjects.

To minimize association biases and because features might exhibit a significance in a multilinear model despite not showing any real correlation in a bivariate analysis, we fitted three multilinear models (Table 1). Model 1 focused on demographic parameters only, and there was a significant effect of ethnicity such that black and Chinese participants revealed a positive correlation to macular curvature scores. Age and sex revealed a significant effect, as well, which changed distinctively in the models 2 and 3, which included functional and ocular measures and infancy factors, respectively. In addition to ethnicity, refractive error consistently revealed the most significant effect on macular curvature scores. The impact of VA, corneal curvature, IOP, FI, and birthweight was low, but still significant. Maternal smoking, however, did not reveal any significance in the model.

Dome-Shaped Configuration

Defined as inverted macular curvature (negative values) (Fig. 2), the prevalence of a macular dome-shaped configuration was overall 4.78% (6040 eyes of 4725 subjects) and was more common in hypermetropic than in emmetropic or myopic eyes (Table 2). Of note, the prevalence increased with more extreme refractive errors into both directions. In contrast, an extensive dome-shaped macular configuration (fourth quartile of eyes with negative macular curvature values; macular curvature, <−0.00105589; 1.26%; 1599 eyes of 1346 subjects) was more common in myopic than in emmetropic or hypermetropic eyes. The highest prevalence of this particular extensive macular shape was found in the subgroup of high myopia (Table 2), in particular in the subset of those eyes with very high refractive error (<−9 diopters spherical equivalent), which revealed a prevalence of 6.49% (79 of 1217 eyes). The odds ratios for the extensive macular dome-shaped configuration were 3.23 and 5.34 for high and very high myopia, respectively. In the set of the 100 eyes with the most negative macular curvature (i.e., most extensive macular dome-shaped configuration), subretinal fluid was present in 29% of cases, whereas it was absent in all other assessed OCT scans (used for validation), including those with negative macular curvature. The 100 eyes with the most negative macular curvature revealed significantly impaired VA compared to other eyes (mean ± SD, 0.140 ± 0.212 vs. 0.020 ± 0.202; $P < 0.0001$), whereas those with and without subretinal fluid did not show a significant difference in VA ($P = 0.344$).

In terms of ethnicity, a macular dome-shaped and an extensive dome-shaped configuration were most common in subjects of Chinese origin (5.38% and 2.15%, respectively) followed by white origin (4.99% and 1.33%, respectively) and other origin (3.86% and 0.96%, respectively). Subjects

Table 1. Standard Deviation Differences in Macular Curvature by Change in Independent Variables

	Model 1			Model 2			Model 3		
Independent Variables	**Estimates**	**CI**	***P***	**Estimates**	**CI**	***P***	**Estimates**	**CI**	***P***
Age (per decade)	–0.05	–0.06 to –0.05	**1.3E-32**	0.04	0.04–0.05	**5.6E-20**	0.02	0.01–0.04	**1.1E-04**
Sex									
Female (ref.)	—	—	—	—	—	—	—	—	—
Male	0.02	0.01–0.04	**5.1E-03**	–0.01	–0.02 to 0.01	3.3E-01	–0.03	–0.05 to –0.01	**1.1E-02**
Ethnicity									
White (ref.)	—	—	—	—	—	—	—	—	—
Black	0.14	0.10–0.18	**1.6E-10**	0.23	0.18–0.27	**7.7E-21**	0.14	0.06–0.22	**1.1E-03**
Asian	0.002	–0.04 to 0.04	9.4E-01	0.07	0.03–0.12	**2.3E-03**	0.07	–0.01 to 0.15	7.5E-02
Other	0.002	–0.05 to 0.05	9.4E-01	0.11	0.05–0.18	**2.0E-04**	0.12	0.03–0.22	**1.4E-02**
Mixed	0.04	–0.03 to 0.12	2.8E-01	0.05	–0.04 to 0.13	2.8E-01	0.03	–0.09 to 0.14	6.6E-01
Chinese	0.40	0.29–0.50	**1.1E-12**	0.21	0.09–0.33	**7.6E-04**	0.08	–0.10 to 0.26	3.6E-01
Visual acuity (per 0.1 logMAR)	—	—	—	–0.02	–0.02 to –0.01	**8.4E-36**	–0.02	–0.02 to –0.01	**1.8E-21**
Refractive error (per D)	—	—	—	–0.15	–0.15 to –0.15	**0.0E+00**	–0.15	–0.16 to –0.15	**0.0E+00**
Corneal curvature (per D)	—	—	—	–0.02	–0.03 to –0.02	**2.2E-19**	-0.02	–0.03 to –0.02	**1.7E-13**
Intraocular pressure (per mmHg)	—	—	—	–0.02	–0.03 to –0.02	**3.8E-14**	–0.02	–0.03 to –0.02	**8.2E-09**
Fluid intelligence	—	—	—	0.03	0.03–0.03	**4.6E-63**	0.03	0.03–0.04	**1.9E-40**
Maternal smoking	—	—	—	—	—	—	0.02	0.00–0.004	7.3E-02
Birthweight (per kg)	—	—	—	—	—	—	–0.03	–0.05 to –0.02	**4.8E-05**

Model 1 was a multilevel model that adjusted for demographic parameters (age, sex, and ethnicity) as fixed effects and a random effect for person to allow for within-person eye measurements. Model 2 was an adjusted version of model 1 that included functional measures (visual acuity and fluid intelligence) and ocular measures (spherical equivalent, corneal curvature, and intraocular pressure). Model 3 was an adjustment of model 2 that included infancy factors (maternal smoking and birthweight). The marginal R^2 values (i.e., variance explained by the models) and the conditional R^2 values were 0.004 and 0.747 for model 1, 0.161 and 0.794 for model 2, and 0.167 and 0.797 for model 3, respectively. P-values < 0.05 were considered significant and indicated by bold figures.

Table 2. Dome-Shaped Macular Configuration and Refractive Error

		Dome-Shaped Configuration (*N* = 6040)		**Extensive Dome-Shaped Configuration (*N* = 1599)**	
Refractive Subgroup	***N***	**%**	***n***	**%**	***n***
Emmetropia	58,432	3.17	1855	0.74	435
Hypermetropia	33,283	7.37	2453	1.43	475
Mild	25,843	5.43	1404	1.19	308
Moderate	6317	12.70	802	2.09	132
High	1123	21.99	247	3.12	35
Myopia	34,576	5.01	1732	1.99	689
Mild	17,279	4.06	702	1.52	262
Moderate	12,355	5.14	635	1.95	241
High	4943	7.99	395	3.76	186

with Asian (2.74% and 0.60%, respectively), mixed (2.44% and 0.72%, respectively), or black (1.90% and 0.41%, respectively) origin showed the particular concave macular configuration less frequently. These findings were partly independent from the impact of refraction on macular curvature, as Chinese subjects had a significantly higher proportion of dome-shaped macular presentation in each refraction subgroup excluding moderate and high hypermetropia (which was absent in our Chinese cohort) compared to other ethnicities; for example, in the high myopia subgroup, Chinese represented 8.54% and white 8.39%. This difference became even more obvious in the group of those with extensive dome-shaped macular configurations; for example, in the high myopia subgroup, Chinese represented 6.10% and white 3.94%. For this phenotype, the odds ratios for Chinese subjects with high or very high myopia were 4.83 and 7.91, respectively.

Inter-Eye Comparison

In 61,319 subjects (33,158 female) with a mean age of 57.2 ± 8.11 years (range, 39.2–70.5) both eyes were included in this study. Inter-eye comparison revealed small but significant differences in macular curvature (OD, 0.00214 ± 0.00144; OS, 0.00213 ± 0.00143; $P = 0.012$), refractive error (OD, −0.339 ± 2.640 D; OS, −0.280 ± 2.670 D; $P < 0.001$), VA (OD, 0.021 ± 0.199 logMAR; OS, 0.018 ± 0.204 logMAR; $P = 0.003$), and IOP (OD, 16.0 ± 4.18; OS, 15.9 ± 4.22; $P < 0.001$). Nevertheless, all parameters showed a high inter-eye correlation (Supplementary Fig. S3). In this cohort, the prevalence of macular dome-shaped and extensive dome-shaped configurations was similar to the aforementioned overall study population with values of 4.67% (5723 eyes of 4327 participants) and 1.20% (1467 eyes of 1187 participants), including a binocular manifestation in 32.26% and 23.59% of subjects, respectively. In the majority of participants with monocular manifestation, the affected eye was more hypermetropic or less myopic (65.50% and 54.10% for dome-shaped and extensive dome-shaped macular configurations, respectively).

Discussion

The unique dataset contained within the UKBB has allowed systematic and comprehensive investigation of the macular morphology including curvature in the largest cohort to date. We found that demographic, ocular, functional, and infancy parameters were associated with macular curvature, whereas refractive error and ethnicity were the most significant factors.

In our cohort, the six ethnicity groups we investigated showed different refractive errors; however, the effects of ethnicity on macular curvature were not explained by these differences alone. Among others, black and Chinese ethnicity consistently showed a likewise effect on macular curvature while presenting different extremes of refractive error

(Fig. 3). Furthermore, the effect of ethnicity stayed significant or even increased in the multivariate model 2, which included ocular measures such as refractive error (Table 1). Last, the odds ratio for the dome-shaped configuration was higher in Chinese subjects than in the general cohort, even when categorized into similar refractive error subgroups.

Myopia was generally associated with higher macular curvature values. A Mendelian randomization analysis in the UKBB has shown that every additional year spent in education resulted in a more myopic refractive error (−0.27 D/y), whereas myopic status itself does not affect education duration.[30] In this context, it is interesting to note that a consistent positive association between macular curvature and fluid intelligence was found (Fig. 3). It may therefore be hypothesized that some of the associations found between refraction and macular curvature could partly be explained by exposure to more years in education (e.g., posterior pole extension triggered by reading). This might be worth further investigations in the view of increasing myopia prevalence and research interest.[36]

It has been reported that maternal smoking is associated with intrauterine growth restriction that may cause reduced VA, reduced contrast sensitivity, and hypermetropia.[31] We also found a lower birthweight in the group of participants with a history of maternal smoking (3.26 ± 0.67 kg vs. 3.34 ± 0.64 kg) as well as less myopia (−0.21 ± 2.67 D vs. −0.35 ± 2.68 D), which might account for the lower macular curvature measures in this group (Fig. 3). A birthweight less than the 10th percentile is known to be a risk factor for hypermetropia,[31] which could explain the left wing of the inverted U-shape of the association between birthweight and macular curvature (Fig. 3). The remaining significant negative association is open for further research.

Of particular interest, we focused on the particular dome-shaped configuration that was most frequent in eyes with high refractive error. The highest odds ratio was found for the extensive dome-shaped configuration in Chinese subjects with very high myopia (7.91), whereas the overall dome-shaped configuration was more commonly found in hypermetropic eyes. However, in the initial description of dome-shaped maculopathy by Gaucher and colleagues in 2008,[4] only myopic eyes were reported. Hypothesized causal factors for this particular macular configuration include mechanical parameters, in particular vitreomacular traction and/or low IOP. In particular, it has been suggested that hypotonia is present in the area of staphyloma associated with lower wall tension leading to an inward collapse of the sclera. However, no supporting evidence for this hypothesis could ever be found,[1,32] which is in line with our findings of an only minor and inconstant association between IOP and macular curvature (Fig. 3). Another possible explanation for the dome-shaped configuration is based on a localized area of scleral and choroidal thickening, as an increased macular bulge height has been reported using different imaging technologies.[3,4,6,37] Experiments in chicks have supported this hypothesis, as they revealed that choroidal and scleral thickening at the posterior pole occur in the development of myopia and the recovery after deprivation-induced myopia.[38–40] Further studies revealed an association with general posterior malformation in high myopia, which indicated that the macular dome-shaped configuration might not necessarily be caused by an inward protrusion of the globe but could be due to a possible anatomical preservation at the macula (localized resistance of the sclera to the staphylomatous deformation).[4,33–35] In these cases, the development of a macular dome-shaped configuration could represent an adaptation to reduce the defocus and maintain emmetropization.[3,6,41,42]

It has been reported that scleral and choroidal thinning is more pronounced in the parafoveal area than at the foveal center, resulting in a relative (not absolute) increase in macular bulge height.[33,34] Using three-dimensional magnetic resonance imaging, a recent study supported the hypothesis of a general posterior malformation, as they located the macula within, at the boundary of or between posterior staphylomas in many myopic eye but not in non-myopic dome eyes.[1] Some chick experiments also revealed more generalized anatomical changes of morphology of the posterior globe after optical defocus and form deprivation.[43,44] Of note, a general weakness of connective tissue of the whole eye might be unlikely, given the missing association of macular and corneal curvature in our cohort (Fig. 3) and the fact that other studies have not found a generalized thickened sclera in their cohorts of eyes with the dome-shaped configuration.[3] The increasing prevalence of the dome-shaped configuration with more extreme refractive error, however, might account for some kind of general ocular maldevelopment or malformation.

Other studies have shown that a dome-shaped macular configuration can also be found in subjects with emmetropia and hypermetropia.[3,45] In our cohort, the inverted macular curvature (negative curvature values) was even more common in hypermetropia than in myopia (Table 2). Different hypotheses might explain the discrepancy between ours and the aforementioned studies. Most prior studies focused on patients with posterior staphyloma and/or visual symptoms. Dome-shaped macular configurations in subjects with emmetropia and hypermetropia may be asymptomatic; thus, subjects do not seek medical advice. The unique population cohort nature of the UKBB study, however, gave us the possibility to detect these subjects, as well. Without computational analysis, a mild dome-shaped configuration (more often associated with hypermetropia) might, furthermore, not be noticed by human investigators. In this study, the extensive dome-shaped configuration with obvious inverted curvature was more commonly found in myopia (Table 2). Finally, different underlying pathophysiological mechanisms might account for the diverging presentation of the macular dome-shaped configuration in myopes and non-myopes, and further work is needed. A possible approach to answering these questions might be the analysis of macro- and microstructures, as well as molecular factors in more anterior regions such as the equator and the ora serrata. These investigations might also contribute to our understanding of retinal diseases and their hitherto (partly) unexplained primary localized presentation.

In the dome-shaped macular configuration, a serous detachment over the apex of the dome with a presentation similar to that of central serous chorioretinopathy may develop. It has been suggested that a malfunctioning choroid, as well as an obstruction of choroidal fluid outflow by a thickened sclera, could be a potential cause for the associated subfoveal fluid.[6] Other hypotheses to explain the subfoveal fluid include malfunction of the RPE at the dome.[4] In our cohort, subretinal fluid was detected in only a minor proportion of eyes with the most extensive dome-shaped configuration. This indicates that this pathology and associated causes are unlikely to be a general feature of the dome-shaped configuration itself. Presumably, different pathomechanisms might lead to varying severity of presentation. Of

Investigative Ophthalmology & Visual Science

note, the presence of subretinal fluid itself was not directly associated with impaired VA. A more detailed study of macular curvature in hypermetropic eyes may help to determine whether a dome-shaped configuration is a common anatomical risk factor for both myopic and hypermetropic serous detachment of the retina.

A bilateral macular dome-shaped configuration has been reported in 50% to 78% of cases.[3,4,6] Despite the high inter-eye correlation in our cohort, a binocular manifestation was only observed in 32.26% of subjects; the majority did not show a binocular manifestation (Supplementary Fig. S3). Here, the dome-shaped configuration was also slightly more common in the more hypermetropic eye. We hypothesize that the latter might partly derive from shorter axial length due to the concave macular configuration in dome-shaped eyes. Based on previous publications and our results, not only are the causes of dome-shaped configurations still unclear, but also the uniformity of its origin in different refractive subgroups might be questionable. An investigation into the origins of macular configuration was beyond the scope of this study, but such studies might provide further insights into retinal development and the specific formation of the macula, thus being of particular scientific interest for myopia and maculopathy research. In the context of future studies, the polynomial fit analysis might also be used to investigate foveal configurations, particularly with regard to macular diseases, as well as the detection of pathologies, differential diagnoses, and functional predictions. Here, it might be expected that the described slight association of curvature and VA might become more distinct. Reasons for our findings (Fig. 3) might only be hypothesized. One study described a prevalence of retinal dystrophies with macular dome-shaped configurations of 19.6%, which might account for the trend of more impaired VA with lower macular curvature values. However, the authors state that the high prevalence they observed could also be related to the high rate of myopia in genetic ocular diseases or the tertiary referral nature of their institution.[3]

Although our method does not require any human annotations, the presented segmentation algorithm successfully extracted the target regions from noisy, low-contrast images and or B-scan images in which part of the area of interest was missing or was cropped. Because we collected initial training examples by randomly sampling from the entire dataset, the performance on images of less common anatomical variations, such as eyes with extensive concave/convex macular curvature, was slightly inferior to the performance on images of eyes with more typical anatomy. The performance of both segmentation and the flip detector was improved by adding human annotations to the hard examples. Strengths of this study include the unique large sample size and the use of spectral-domain OCT imaging in the UKBB Eyes and Vision substudy (85,737 of 502,882 subjects). As we investigated macular curvature in the largest cohort to date, weak associations were identified that previously had not been found in smaller datasets.[12–15] A total of 65,023 of 85,737 participants met all inclusion criteria to be included in the analysis. Although not randomized, the large sample size would support the assumption that trends among demographic and ocular factors would hold true for cases that were excluded. Furthermore, an extended validation of the curvature calculations was performed in this study in order to ensure high image quality and correct conclusions. This work might therefore serve as a robust base for future basic research focusing on macular development, malformation, and macular diseases. Future longitudinal analysis to detect possible changes and/or further associations might be warranted in this context. The UKBB consortium is preparing to invite participants to take part in a follow-up study.

Although the large UKBB dataset is a main strength of this study, it also has some limitations. First, the dataset does not include biometry or other axial length measures. Not only have macular changes in high myopia been linked to axial length,[46] but axial length might also interfere with the lateral scan dimensions, leading to distortions and inaccuracies of measures that also affect curvature values.[22,28,29] A recent paper showed a reversal of correlation between foveal avascular zone and aging in children by correction for axial length in this context.[47] However, the lateral distortion in our images should have led to fewer (positive or negative) curvature measures in longer eyes and vice versa in shorter eyes and should not have changed the direction of the curvature. It therefore should not alter the main conclusions of our analysis. Other sources of distortion are the unknown relative eye positions, optics of the OCT device, and varying optical paths that are much more difficult to predict. As corrections were not possible, the described associations should be carefully interpreted and not considered as absolute truth. Further limitations of the study include the OCT scan pattern. The analysis was based on horizontal OCT B-scans, so we did not document the vertical oval-shaped dome pattern previously described.[48] The 6-mm volume scan may also not be long enough to determine staphyloma, which might be of particular interest in this context. Also, given the spectral-domain technology of the OCT device and absence of enhanced depth imaging data, choroidal parameters were not included in the analysis but could be of possible importance. Although there was a sampling frame for the UKBB study based on general practitioner patient registers in the UK National Health Service, there is the potential for nonresponse bias, as UKBB participants are likely to be healthier than the general population of the United Kingdom, particularly given the low response rate (5.5%). We did not exclude ocular diseases even if they might have an impact on the macular curvature (e.g., ocular neoplasia), as we aimed to present a representative cross-section of the study cohort. Given the use of our analysis model to calculate macular curvature and the exceptionally large sample size, any possible interfering effect of outer retinal changes was minimized.

Conclusions

This project investigated macular curvature based on OCT images using the unique imaging dataset of the UKBB study, the world's largest cohort study of adults. Refractive error and ethnicity were found to be the most significant determinants of macular curvature, whereas demographic parameters, ocular factors, and childhood environment were found to also have a distinct impact, as well. Of particular interest to the study of eye development, macular diseases, and malformations, this analysis of the dome-shaped macular configuration revealed that this particular presentation of the posterior pole is significantly more common than reported before, especially in emmetropic and hypermetropic eyes. Indeed, it was more commonly found in eyes with high refractive error but does not essentially imply a maculopathy. Despite the limitations of this analysis (e.g., uncorrected distortions of the OCT scan), our findings offer further insights into

Investigative Ophthalmology & Visual Science

the presentation of and potential associations of patients with marked concave and convex macular configurations. It also provides evidence of the multiple pathophysiologic processes leading to the specific formations, offering new directions for future myopia and macula research.

Acknowledgments

Supported by grants from the German Research Foundation (MU4279/2-1 to PLM); Mexican National Council of Science and Technology (to AOB); Wellcome Trust (220558/Z/20/Z to ANW); National Eye Institute, National Institutes of Health (K23EY029246 to AYL); Lantham Vision Innovation Award (to AYL); and Research to Prevent Blindness (to AYL), in addition to support from the National Institute for Health Research Biomedical Research Centre based at Moorfields Eye Hospital NHS Foundation Trust and UCL Institute of Ophthalmology (to AT and CE) and the Special Trustees of Moorfields Eye Hospital (to UK Biobank Eye and Vision Consortium). The views expressed are those of the authors and not necessarily those of the National Health Service, National Institute for Health Research, Department of Health, or the U.S. Food and Drug Administration. The funder had no role in the design and conduct of the study; collection, management, analysis, and interpretation of the data; preparation, review, or approval of the manuscript; and decision to submit the manuscript for publication.

Disclosure: **P.L. Müller,** None; **Y. Kihara**, None; **A. Olvera-Barrios**, None; **A.N. Warwick**, None; **C. Egan**, Heidelberg Engineering (C, R), Novartis Pharmaceuticals (F); **K.M. Williams**, None; **A.Y. Lee**, Santen (F), U.S. Food and Drug Administration (R), Genentech (C, R), Gyroscope (R), Carl Zeiss Meditec (F), Topcon (F), Microsoft (R), Johnson & Johnson (C, R); **A. Tufail**, Allergan (C, R), Bayer (F, C, R), Kanghong (R), Heidelberg Engineering (C, R), Novartis (F, C, R), Roche/Genentech (C, R), Iveric Bio (C, R), Apellis (C, R), Thea (C, R)

References

1. Dai F, Li S, Wang Y, et al. Correlation between posterior staphyloma and dome-shaped macula in high myopic eyes. *Retina*. 2020;40(11):2119–2126.
2. Lichtwitz O, Boissonnot M, Mercié M, Ingrand P, Leveziel N. Prevalence of macular complications associated with high myopia by multimodal imaging. *J Fr Ophtalmol*. 2016;39(4):355–363.
3. Errera M-H, Michaelides M, Keane PA, et al. The extended clinical phenotype of dome-shaped macula. *Graefes Arch Clin Exp Ophthalmol*. 2014;252(3):499–508.
4. Gaucher D, Erginay A, Lecleire-Collet A, et al. Dome-shaped macula in eyes with myopic posterior staphyloma. *Am J Ophthalmol*. 2008;145(5):909–914.e1.
5. Hainsworth DP, Sommerville DN, Ranson NT, Todd KC, Gigantelli JW. Bruch's membrane abnormalities in dome-shaped and mushroom-shaped choroidal melanomas. *Ann Acad Med Singapore*. 2006;35(2):87–88.
6. Imamura Y, Iida T, Maruko I, Zweifel SA, Spaide RF. Enhanced depth imaging optical coherence tomography of the sclera in dome-shaped macula. *Am J Ophthalmol*. 2011;151(2):297–302.
7. Ueda E, Yasuda M, Fujiwara K, et al. Five-year incidence of myopic maculopathy in a general Japanese population. *JAMA Ophthalmol*. 2020;138(8):887.
8. World Health Organization. *The Impact of Myopia and High Myopia: Report of the Joint World Health Organisation–Brian Holden Vision Institute Global Scientific Meeting on Myopia*. Geneva, Switzerland: World Health Organization; 2015.
9. Jan CL, Congdon N. Chinese national policy initiative for the management of childhood myopia. *Lancet Child Adolesc Health*. 2018;2(12):845–846.
10. Yan YN, Wang YX, Yang Y, et al. Ten-year progression of myopic maculopathy. *Ophthalmology*. 2018;125(8):1253–1263.
11. Müller PL, Wolf S, Dolz-Marco R, Tafreshi A, Schmitz-Valckenberg S, Holz FG. Ophthalmic diagnostic imaging: retina. In: Bille JF, ed. *High Resolution Imaging in Microscopy and Ophthalmology: New Frontiers in Biomedical Optics*. Cham: Springer International Publishing; 2019:87–106.
12. Minami S, Ito Y, Ueno S, et al. Analysis of macular curvature in normal eyes using swept-source optical coherence tomography. *Jpn J Ophthalmol*. 2020;64(2):180–186.
13. Koyanagi Y, Ueno S, Ito Y, et al. Relationship between macular curvature and common causative genes of retinitis pigmentosa in Japanese patients. *Invest Ophthalmol Vis Sci*. 2020;61(10):6.
14. Meinert M, Ueno S, Komori S, et al. Longitudinal changes of macular curvature in patients with retinitis pigmentosa. *Transl Vis Sci Technol*. 2020;9(10):11.
15. Komori S, Ueno S, Ito Y, et al. Steeper macular curvature in eyes with non-highly myopic retinitis pigmentosa. *Invest Ophthalmol Vis Sci*. 2019;60(8):3135.
16. Allen N, Sudlow C, Downey P, et al. UK Biobank: current status and what it means for epidemiology. *Health Policy Technol*. 2012;1(3):123–126.
17. Palmer LJ. UK Biobank: bank on it. *Lancet*. 2007;369(9578):1980–1982.
18. Ollier W, Sprosen T, Peakman T. UK Biobank: from concept to reality. *Pharmacogenomics*. 2005;6(6):639–646.
19. Cumberland PM, Bao Y, Hysi PG, Foster PJ, Hammond CJ, Rahi JS. Frequency and distribution of refractive error in adult life: methodology and findings of the UK Biobank Study. *PLoS One*. 2015;10(10):e0139780.
20. Flaxman SR, Bourne RRA, Resnikoff S, et al. Global causes of blindness and distance vision impairment 1990-2020: a systematic review and meta-analysis. *Lancet Glob Health*. 2017;5(12):e1221–e1234.
21. Patel PJ, Foster PJ, Grossi CM, et al. Spectral-domain optical coherence tomography imaging in 67 321 adults: associations with macular thickness in the UK Biobank Study. *Ophthalmology*. 2016;123(4):829–840.
22. Kuo AN, Liu A, Wong CW, et al. Curvature differences in myopic eyes with and without staphyloma using OCT. *Invest Ophthalmol Vis Sci*. 2019;60(9):4356.
23. Hart P, Nilsson N, Raphael B. A formal basis for the heuristic determination of minimum cost paths. *IEEE Trans Syst Sci Cybern*. 1968;4(2):100–107.
24. Dijkstra EW. A note on two problems in connexion with graphs. *Numer Math*. 1959;1(1):269–271.
25. Zhao H, Shi J, Qi X, Wang X, Jia J. Pyramid scene parsing network. In: *Proceedings of the IEEE Conference on Computer Vision and Pattern Recognition*. Piscataway, NJ: Institute of Electrical and Electronics Engineers; 2016:2881–2890.
26. He K, Zhang X, Ren S, Sun J. Deep residual learning for image recognition. In: *Proceedings of the IEEE Conference on Computer Vision and Pattern Recognition*. Piscataway, NJ: Institute of Electrical and Electronics Engineers; 2015:770–778.
27. Le Cun Y, Boser B, Denker JS, et al. Handwritten digit recognition with a back-propagation network. In: Lisboa PGJ, ed. *Neural Networks: Current Applications*. Boca Raton, FL: Chapman & Hall; 1992:396–404.
28. Kuo AN, Verkicharla PK, McNabb RP, et al. Posterior eye shape measurement with retinal OCT compared

Investigative Ophthalmology & Visual Science

to MRI. *Invest Ophthalmol Vis Sci*. 2016;57(9):OCT196–OCT203.
29. Montesano G, Ometto G, Hogg RE, Rossetti LM, Garway-Heath DF, Crabb DP. Revisiting the Drasdo model: implications for structure-function analysis of the macular region. *Transl Vis Sci Technol*. 2020;9(10):15.
30. Mountjoy E, Davies NM, Plotnikov D, et al. Education and myopia: assessing the direction of causality by mendelian randomisation. *BMJ*. 2018;361:k2022.
31. Lindqvist S, Vik T, Indredavik MS, Brubakk A-M. Visual acuity, contrast sensitivity, peripheral vision and refraction in low birthweight teenagers. *Acta Ophthalmol Scand*. 2006;85(2):157–164.
32. Mehdizadeh M, Nowroozzadeh MH. Author reply: dome-shaped macula in eyes with myopic posterior staphyloma. *Am J Ophthalmol*. 2008;146(3):478–479.
33. Soudier G, Gaudric A, Gualino V, et al. Macular choroidal thickness in myopic eyes with and without a dome-shaped macula: a case-control study. *Ophthalmologica*. 2016;236(3):148–153.
34. Ellabban AA, Tsujikawa A, Muraoka Y, et al. Dome-shaped macular configuration: longitudinal changes in the sclera and choroid by swept-source optical coherence tomography over two years. *Am J Ophthalmol*. 2014;158(5):1062–1070.e2.
35. Ellabban AA, Tsujikawa A, Matsumoto A, et al. Three-dimensional tomographic features of dome-shaped macula by swept-source optical coherence tomography. *Am J Ophthalmol*. 2013;155(2):320–328.e2.
36. Agarwal D, Saxena R, Gupta V, et al. Prevalence of myopia in Indian school children: meta-analysis of last four decades. *PLoS One*. 2020;15(10):e0240750.
37. Soudier G, Gaudric A, Gualino V, et al. Long-term evolution of dome-shaped macula. *Retina*. 2016;36(5):944–952.
38. Gottlieb MD, Joshi HB, Nickla DL. Scleral changes in chicks with form-deprivation myopia. *Curr Eye Res*. 1990;9(12):1157–1165.
39. Christensen AM, Wallman J. Evidence that increased scleral growth underlies visual deprivation myopia in chicks. *Invest Ophthalmol Vis Sci*. 1991;32(7):2143–2150.
40. Rada JA, Matthews AL, Brenza H. Regional proteoglycan synthesis in the sclera of experimentally myopic chicks. *Exp Eye Res*. 1994;59(6):747–760.
41. Keane PA, Mitra A, Khan IJ, Quhill F, Elsherbiny SM. Dome-shaped macula: a compensatory mechanism in myopic anisometropia? *Ophthalmic Surg Lasers Imaging*. 2012;43(Online):e52–e54.
42. Norman RE, Flanagan JG, Rausch SMK, et al. Dimensions of the human sclera: thickness measurement and regional changes with axial length. *Exp Eye Res*. 2010;90(2):277–284.
43. Ehrlich D, Sattayasai J, Zappia J, Barrington M. Effects of selective neurotoxins on eye growth in the young chick. *Ciba Found Symp*. 2007;155:63–84.
44. Beresford JA, Crewther SG, Crewther DP. Anatomical correlates of experimentally induced myopia. *Aust N Z J Ophthalmol*. 1998;26:S84–S87.
45. Kedkovid N, Afshar AR, Damato BE, Stewart JM. Dome-shaped macula with thickened choroid in an emmetropic patient. *Retin Cases Brief Rep*. 2015;9(4):307–310.
46. Holden BA, Fricke TR, Wilson DA, et al. Global prevalence of myopia and high myopia and temporal trends from 2000 through 2050. *Ophthalmology*. 2016;123(5):1036–1042.
47. Linderman RE, Heffernan E, Ferrante S, Bachman-Groth J, Carroll J. The impact of axial eye growth on foveal avascular zone measurements in children. *Optom Vis Sci*. 2022;99(2):127–136.
48. Caillaux V, Gaucher D, Gualino V, Massin P, Tadayoni R, Gaudric A. Morphologic characterization of dome-shaped macula in myopic eyes with serous macular detachment. *Am J Ophthalmol*. 2013;156(5):958–967.e1.